Spatial organization and evolution period of the epidemic model using cellular automata

Quan-Xing Liu,* Zhen Jin,† and Mao-Xing Liu
Department of Mathematics, North University of China, Taiyuan, Shan'xi 030051, People's Republic of China
(Received 12 May 2006; revised manuscript received 3 June 2006; published 13 September 2006)

We investigate epidemic models with spatial structure based on the cellular automata method. The construction of the cellular automata is from the study by Weimar and Boon about the reaction-diffusion equations [Phys. Rev. E **49**, 1749 (1994)]. Our results show that the spatial epidemic models exhibit the spontaneous formation of irregular spiral waves at large scales within the domain of chaos. Moreover, the irregular spiral waves grow stably. The system also shows a spatial period-2 structure at one dimension outside the domain of chaos. It is interesting that the spatial period-2 structure will break and transform into a spatial synchronous configuration in the domain of chaos. Our results confirm that populations embed and disperse more stably in space than they do in nonspatial counterparts.

DOI: 10.1103/PhysRevE.74.031110 PACS number(s): 05.50.+q, 87.23.Cc, 87.18.Hf, 89.75.Fb

INTRODUCTION

Several theoretical models have shown that population invasion and dispersion is more stable in space than that in nonspatial counterparts. More stable means that a previously unstable equilibrium point becomes stable under a greater variety of conditions, or that an equilibrium is approached faster [1]. In oscillatory systems where the equilibrium is a limit cycle or more generally, an unstable focus, diffusion or dispersal will create wavelike patterns. The lattice Lotka-Volterra (LLV) model was studied extensively [2–4]. In a nonlinear ecology system, the two most commonly seen patterns are spiral waves and turbulence. Spiral waves play an important role in ecological systems. For example, spatially induced speciation prevents the extinction of the predator-prey models [5,6]. A classical epidemic model is an ordinary differential equation (ODE) or a mean-field (MF) approximation [7]. The ODE methods (or MF) are based on the assumption that the population is well mixed, with the subpopulations (involving susceptible, infected, removed, etc.), interacting in proportion to their sizes. Nonspatial theory typically predicts a selection for the maximal number of secondary infectors. Among these epidemic features, the existence of threshold values is crucial for the spread of an infection [8,9]. A second classical approach describes spatially extended subpopulations such as a coupled map-lattice model [10], reaction-diffusion equations, deterministic cellular automata, and an integrodifference equations model. In the literature [11] the authors present the numerical simulations in a predator-prey system, and show that there are either irregular spatiotemporal oscillations behind the invasion or regular spatiotemporal oscillations with the form of a periodic traveling "wake" depending on parameter values.

In our paper, the geographic spread of an epidemic can be analyzed as a reaction-diffusion system in which both the subpopulation exhibits local random movement and the algorithm of cellular automata are based on this paper [11,12]. More recently, studies have shown large-scale spatiotemporal patterns in measles [13] and dengue fever [14]. These studies have shed new light onto key research issues in spatial epidemic dynamics, but the detailed theoretical studies are difficult. The study of population dynamics takes into account the species distribution in space, interactions between individual species that are located in the same neighborhood, and the mobility of the various species [15–17]. These studies predict the formation of a spatial complex structure, phase transitions, multistability, oscillatory regions, etc. In Ref. [17], the author studies the susceptible-infected–resistant-susceptible (SIRS) models with a spatial structure using cellular automata rules, showing the formation process of the spatial patterns (turbulent waves and stable spiral waves) in the two-dimensional space and the existence of stable spiral waves in the SIRS model.

The principal objective of the present work is that the susceptible-exposed–infected-resistant (SEIR) model with spatial structure is investigated by using the cellular automata algorithm. The SEIR model and its classical ODE version are presented in Refs. [18,19]. In fact, many diseases are seasonal, and therefore an important question for further study is how seasonality can influence spatial epidemic spread and evolution. Hence, we consider the seasonal parameter $\beta(t)=\beta_0[1+\varepsilon \sin(2\pi t)]$, where ε is the fluctuating amplitude of the contact rate. Commonly, we describe the susceptibility, exposure, infection, and recover process in terms of four nonlinear ODEs. We use S for susceptibles, E for the exposed, I for infectors, and R for the recovered. The dynamical equations for the SEIR model are

$$\frac{dS}{dt} = \mu(1-S) - \beta(t)IS, \tag{1a}$$

$$\frac{dE}{dt} = \beta(t)IS - (\mu+\delta)E, \tag{1b}$$

$$\frac{dI}{dt} = \delta E - (\gamma+\mu)I, \tag{1c}$$

*Electronic address: liuqx315@sina.com
†Electronic address: jinzhn@263.net

$$\frac{dR}{dt} = \gamma I - \mu R. \tag{1d}$$

Here μ is the death rate per capacity, and $1/\delta$ and $1/\gamma$ are the mean latent and infectious periods, respectively, of the disease. $\beta(t)$ is the rate of disease transmission between individuals. The population can be normalized to $S+E+I+R=1$, so all dependent variables represent fractions of the population. The original studies show that the system of (1) exists with three phase transitions, which are the stable behavior, the limit cycle, and the chaotic behavior in the mean-field limit [18] with respect to the fluctuating amplitude ε.

NEIGHBORHOOD-DEPENDENT MODEL

Generally, studies on the spatial epidemic models show that there exists spatiotemporal traveling waves [20] [e.g., dengue hemorrhagic fever (DHF) [14,21] and measles [13]]. However, few systems are well enough documented to detect repeated waves and to explain their interaction with spatiotemporal variations in population structure and demography. The actual epidemic spread is spatiotemporal and local individuals interact. Here we study the individual moving of the susceptible, exposed, infector, and recover models, and their diffusion from one lattice site to another. Then Eqs. (1) read

$$\frac{\partial S(r,t)}{\partial t} = \mu - \beta(t) IS - \mu S + D_1 \nabla^2 S(r,t), \tag{2a}$$

$$\frac{\partial E(r,t)}{\partial t} = \beta(t) IS - (\mu + \delta) E + D_2 \nabla^2 E(r,t), \tag{2b}$$

$$\frac{\partial I(r,t)}{\partial t} = \delta E - (\gamma + \mu) I + D_3 \nabla^2 I(r,t), \tag{2c}$$

$$\frac{\partial R(r,t)}{\partial t} = \gamma I - \mu R + D_4 \nabla^2 R(r,t). \tag{2d}$$

We study the system (2) using the cellular automata method, which is suitable for modeling many reaction-diffusion systems in a quantitatively correct way based on Ref. [12], and demonstrate recurrent epidemic spiral waves or traveling waves in an exhaustive spatiotemporal system through the numerical simulation. Simply, we use $c(r,t)$ to denote the vector of individual density in position r and at time t, and $L(c(r,t))$ to describe the local kinetics; D is the diffusion coefficient matrix. Then the system (2) can be written as

$$\frac{\partial c(r,t)}{\partial t} = L(c(r,t)) + D\nabla^2 c(r,t). \tag{3}$$

In the following simulation, we may discard Eq. (2d) since we are concerned only with the susceptible, exposed, and infected models.

We define this model as follows. Space is made up of a square lattice of $J \times J$. In each step the individuals randomly move in its neighborhood. The state of the cellular automata is given by a regular array of density vector c residing on a two-dimensional lattice. We consider cellular automata with b_i states (denoted by the integers $0,1,2,3,\ldots,b_i$). Here species states 0 and b_i are zero population level and maximum population level, respectively. The first step of each time iteration corresponds to local dynamics and the state at each spatial lattice changes independently of the states at other vicinity lattices. The second part of each time step corresponds to unbiased spatial movement. The central operation of the cellular automaton consists of calculating the sum

$$c_i(r,t) = \sum_{r' \in N_i} c_i(r+r'), \tag{4}$$

where the summation takes up all of the nearest neighbors of the cell r. The neighborhoods can be different for each species i. We use the Moore neighborhood for all i in the two-dimensional space, i.e.,

$$N_{square} = \{(0,0),(1,0),(0,1),(-1,0),(0,-1), (1,1),(-1,1),(1,-1),(-1,-1)\}. \tag{5}$$

We normalize the values of $c_i(r,t)$, and the $\bar{c}_i(r,t) = c_i(r,t)/(b_i N_i)$ is the local average density of the $c_i(r,t)$. The $\bar{c}_i(r,t)$ is always between zero and one.

From Ref. [12], the two-dimensional discretization version of Eq. (3) takes the form

$$c_i(r,t+1) = c_i(r,t) + \Delta t L(c_i(r,t)) + D_i \nabla^2 c_i(r,t), \quad i = 1,2,3,4, \tag{6}$$

where

$$D_i = D_{ii} \frac{\Delta t}{\Delta r^2}, \quad i = 1,2,3,4, \tag{7}$$

and D_i defines the space scale.

Furthermore, we have

$$c_i(r,t+1) = L^*(\bar{c}_i(r,t)), \quad i = 1,2,3,4, \tag{8}$$

where $L^*(\bar{c}_i(r,t)) = \bar{c}_i(r,t) + \Delta t L(\bar{c}_i(r,t))$.

As $c(r,t)$ is the average output of the cellular automata (CA) for the system (2), it is given by

$$c_j(r,t+1) = \left\lfloor b_j L^* \left(\frac{c_i(r,t)}{b_i N_i} \right) \right\rfloor + 1, \tag{9}$$

for species j. A detailed description of $c(r,t)$ as an output of the CA can be found in Ref. [12].

NUMERICAL RESULTS

We have performed extensive numerical simulations of the described model, and the qualitative results are shown here. In cellular automata simulation, periodic boundary conditions are used and $\Delta t = 0.005$. The space scales $D_1 = 0.2$, $D_2 = 0.05$, $D_3 = 0.02$ and the grid size used in the evolutional simulations is 100×100 cells. Every species has 100 states in system (2) and more states enable more accurately for discrete representation of the continuum models, while it is complex for analysis, and this is described in detail

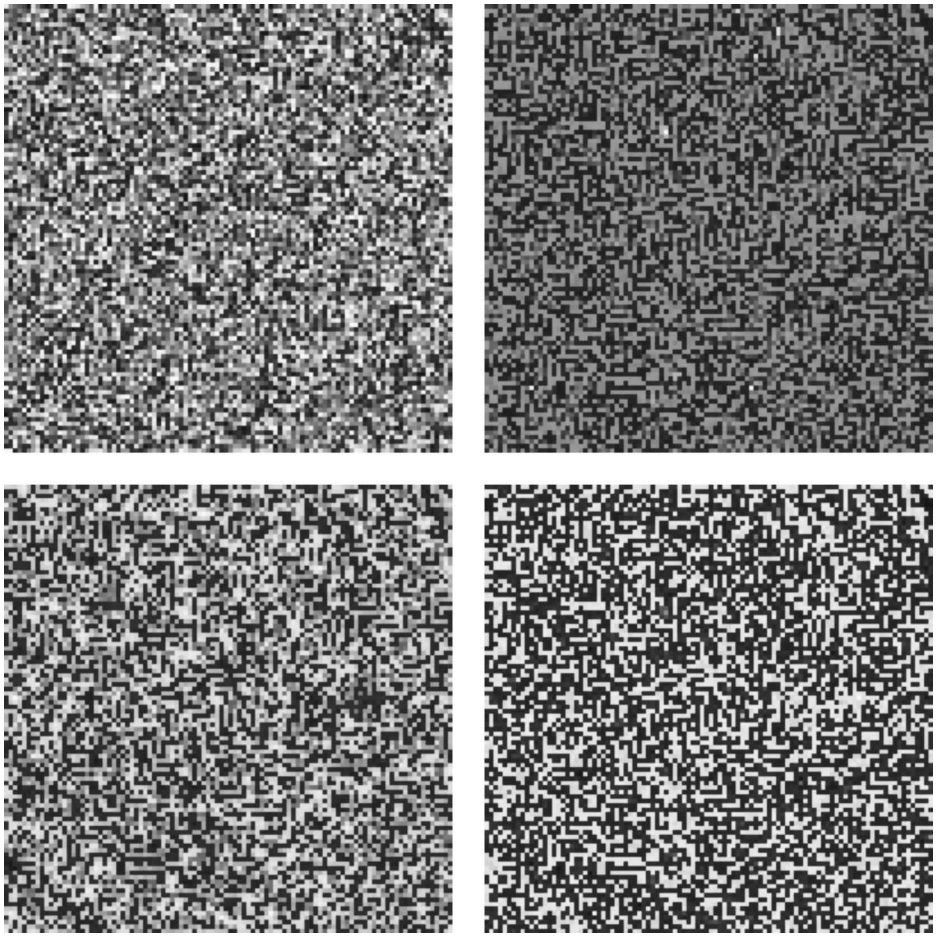

FIG. 1. A typical simulation shows four snapshots of the evolution in two-dimensional space with the parameters $\mu=0.02$, $\delta=35.84$, $\gamma=100$, $\beta_0=1800$, and $\varepsilon=0.23$. The figures plot susceptible density levels as a space on gray scale. The exposed and infected distribution has a qualitatively similar form.

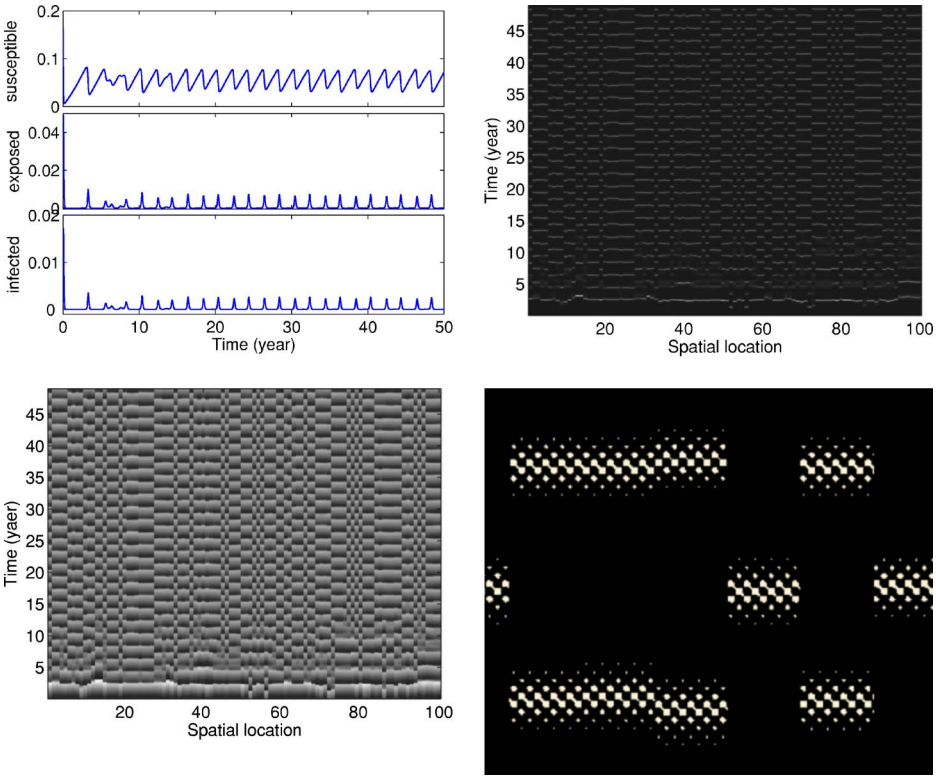

FIG. 2. (Color online) The spatial period-2 structure results for the system (2) in one-dimensional space in cellular automaton models and the parameters are the same as those in Fig. 1. We use a spatial domain of 100 lattices; 10 000 successive time iterations are plotted. In (a) we show the species density as a function of time. (b) and (c) show the susceptible and exposed density levels as a function of space and time on a gray scale, respectively. The behavior of the infected is qualitatively similar. At this scale the spatial discretization is not really visible, and therefore we have enlarged one region of the plane in (c) as in (d), in order to illustrate this discretization.

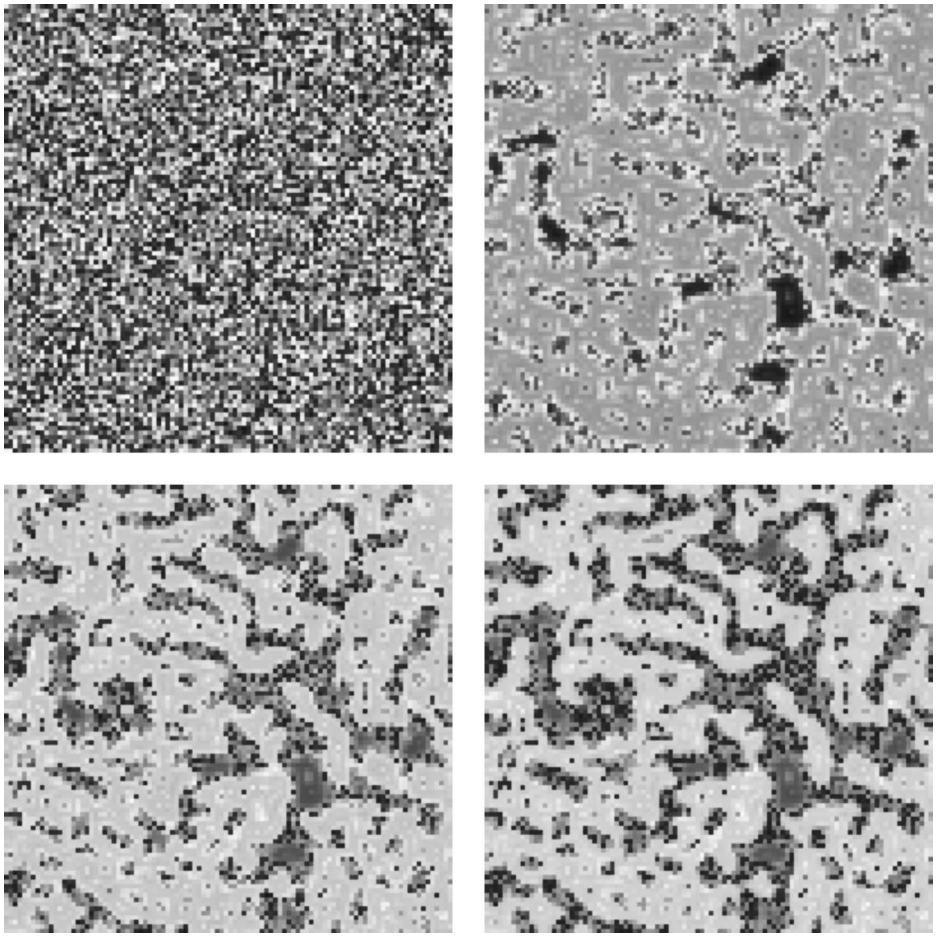

FIG. 3. A typical simulation shows four snapshots of the evolution in two-dimensional space. The parameters are the same as in Fig. 1; $\mu=0.02$, $\delta=35.84$, $\gamma=100$, $\beta_0=1800$, and $\varepsilon=0.38$. The figures plot susceptible density levels as a space on gray scale. The exposed and infected distribution has a qualitatively similar form.

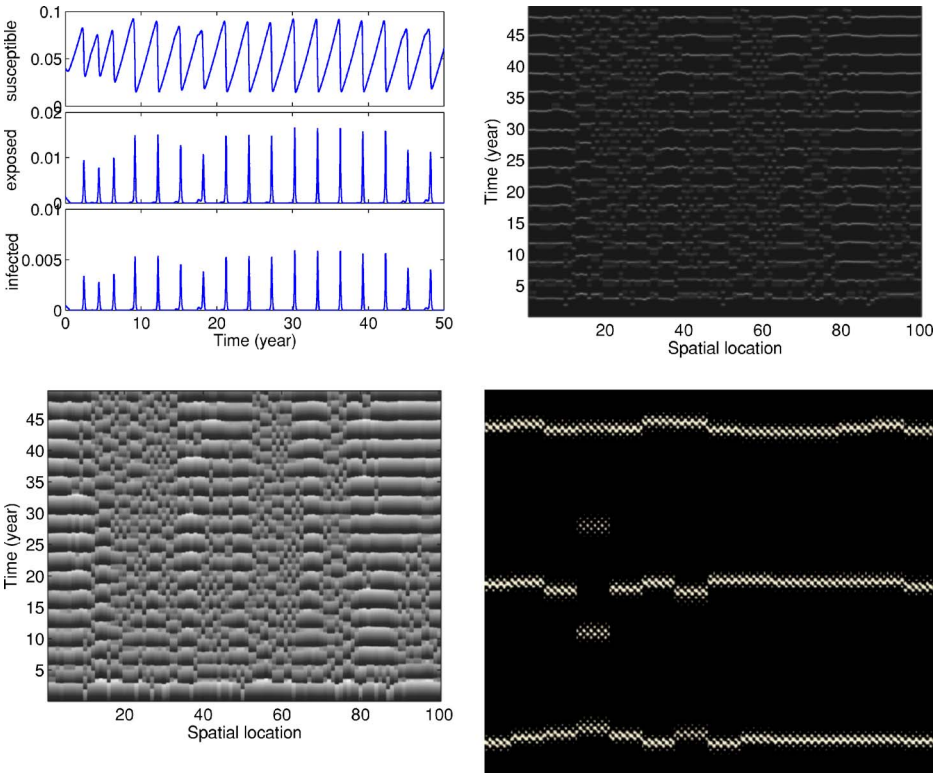

FIG. 4. (Color online) The spatial period-two structure results for the system (2) in one dimension in cellular automata models and the parameters are the same as those in Fig. 3. We use a spatial domain of 100 lattices; 10 000 successive time iterations are plotted. In (a) we show the species density as a function of time. (b) and (c) show the susceptible and exposed density levels as a function of space and time on a gray scale, respectively. The behavior of the infected is qualitatively similar. At this scale the spatial discretization in not really visible, and therefore we have enlarged one region of the plane in (c) as in (d), in order to illustrate this discretization.

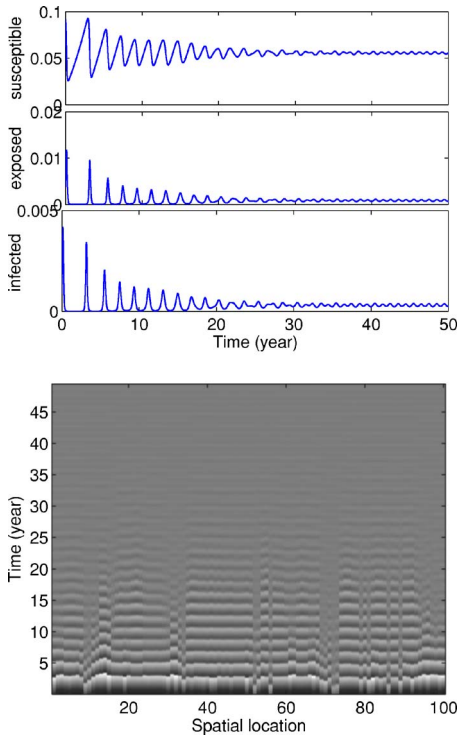

FIG. 5. (Color online) The spatiotemporal evolution of the system (2) in one dimension in cellular automata models for the $\varepsilon < \varepsilon^*$ case, $\varepsilon = 0.035$. In (a) we show the species density as a function of time. (b) is the plot susceptible density as a function of space and time on a gray scale. The behavior of the exposed and infected distribution is qualitatively similar.

elsewhere [22]. We have tested that the larger grid size does not change the qualitative result for the evolutional dynamics. The contact rate fluctuates with the seasons and can be approximated in several ways. Simply we choose sinusoidal force $\beta(t) = \beta_0[1 + \varepsilon \sin(2\pi t)]$, where $0 \leqslant \varepsilon < 1$, and another more realistic option is term-time force, which sets transmission rates high during school terms and low in other places [23]. The spatial patterns evolve from random initial conditions. The maximum density of susceptible levels, exposed levels, and infected levels are set to 50, 5, and 1, respectively, in the two-dimensional space. Other initial conditions have been explored as well, and no change has been observed in the behavior. In Fig. 1 and Fig. 3 four different snapshots during the temporal evolution of the system are presented in two-dimensional space. These figures and the following figures are species density levels as a function of space and time on a gray scale, with white corresponding to the lowest-density state and black corresponding to the highest density state.

Figures 1 and 3 have depicted spatial patterns in the two-dimensional space under different ε values (the fluctuating amplitude of contact rate), respectively. We have examined the temporal evolution by displaying a successive time frame as a movie, but we are unable to represent this effectively on the printed page. From evolution snapshots (Fig. 1), one can see that there is no occurrence of spiral waves (fractal fronts) even if the system reaches a stable state when the ε is in a certain interval. The certain interval turned out to be $\varepsilon^* < \varepsilon < \varepsilon_c$ with the parameter value used in the figure and $\varepsilon^* \approx 0.048$ and $\varepsilon_c \approx 0.305$. Here the critical value $\varepsilon_c \approx 0.305$ in the spatial model (2), which is more than the value of the local dynamic of the chaotic point of system (1) [18] (≈ 0.28). This result suggests another possible explanation, which is that populations embed and disperse more stably in space than they do in nonspatial counterparts [24,25]. As the ε ($\varepsilon > \varepsilon_c$ in the domain of chaos) and time increase, the dynamical patterns with fractal fronts (spirals waves) of spatial structures occur and become larger and more stable (see Fig. 3). The CA models are generally based on qualitative rather than quantitative information about the system. It is difficult to detect the density calculated over the entire lattice when the system is larger. Hence, in order to investigate quantitatively the evolution of system (2), we give the results by one-dimensional space. An explicit visualization of spatial organization within the lattice is provided by the space-time plot of Figs. 2 and 4.

In Fig. 2(a) the three time series displaying the density of susceptible, exposed, and infected models for the first 10 000 steps by CA are given. Self-sustained oscillations of the three time series develop [see Fig. 2(a)]. The amplitude of oscillations increases with the increase of fluctuating amplitude of the infection rate ε [compared Figs. 2(a) and 4(a)]. In fact, large oscillations will lead to the stochastic extinction of the species, when the value of the fluctuating amplitude is more than ε_c in the domain of chaos. In Figs. 2(b) and 2(c), spatiotemporal pictures of the susceptible and exposed models are plotted, respectively, where time increases from bottom to top and the horizontal axis represents the spatial location. From Figs. 2(b) and 2(c), it is clearly seen that the whole system shows the spatial period-two structure when the ε is between ε^* and ε_c (later we will give the case when ε is smaller than a critical value ε^*).

To further investigate the impact of the fluctuating amplitude on the dynamical patterns with fractal fronts (or spiral waves) in two-dimensions and the spatial period-two structure in one-dimensional space, respectively, we study the case when the SEIR model is deeply in the domain of chaos and out of the domain of chaos. The evolution of system (2) is shown with $\varepsilon = 0.38$ in Figs. 3 and 4. In Figs. 3(b)–3(d) three snapshots are taken at 5250, 5300, and 5350 steps, respectively. In Fig. 3(b) the rotating spirals are not recognizable due to the irregular interfaces. However, the spiral formation becomes visible when the interfacial roughness grows by the infected invasion as demonstrated in Fig. 3(d). In Fig. 3(d) one can easily identify the vortices and antivortices rotating clockwise and counterclockwise, respectively. We have to emphasize that this pattern cannot be characterized by a single length unit (e.g., correlation length) because the main features of spirals (armlength, average curvature, average distance, etc.) depend on the model parameters. But, it may be analyzed by using a geometrical features method [26]. The armlengths of these spiral waves are broad and do not easily break, resulting in the periodical recurrence of epidemic waves. The spontaneous formation of spiral waves means the regularly recurrent infection waves [Figs. 3(a)–3(d)]. Similarly, the irregular spiral waves can also be observed even when the fluctuating amplitude is much more than the critical value ε_c. These results are not shown in this paper.

Figure 5 shows the time evolution of the density of the species and the spatiotemporal configurations of the system (2) at $\varepsilon=0.035$. The spatiotemporal evolution of the exposed and infected models are similar to the susceptible's [Fig. 5(b)]. It can be clearly noticed that the spatial period-two structure disappears and the stationary state is a fixed point with the decreasing of ε. The situation corresponds to a low and persistent endemic infection in Fig. 5(a). The oscillations decay to the fixed point when the ε is smaller than the critical value ε^* case. The oscillations decay because these infection clusters grow, the availability of infected hosts per susceptible host is reduced, and the number of new infectors decreases. In this case, the spontaneous formation of dynamical patterns is qualitatively similar in Fig. 3 in two dimensions.

CONCLUSIONS

A realistic spatial epidemic with the individuals randomly moving in its neighborhood has been modeled using cellular automata. Our simulations demonstrate that the recurrent infection waves exist and persist in an exhaustive spatiotemporal system. We have investigated the dynamical patterns of system (2) in one and two dimensions, respectively. We show that the spiral waves recur periodically and the recurrence is insensitive to the change of the fluctuating amplitude ε within the domain of chaos (the fluctuation amplitude $\varepsilon > \varepsilon_c$). Moreover, the dynamical patterns with fractal fronts grow stably. The system also shows a spatial period-2 structure in one dimension when ε is between ε^* and ε_c outside the domain of chaos. It is interesting that the spatial period-two structure will break and transform to spatial synchronous configuration in the domain of chaos. Our results confirm that populations embed and disperse more stably in space than they do in nonspatial counterparts.

ACKNOWLEDGMENTS

This work was supported by the National Natural Science Foundation of China under Grant No. 10471040 and the Science Foundation of Shan'xi Province Grant No. 2006011009.

[1] P. Rohani and O. Miramontes, Proc. R. Soc. London, Ser. B **260**, 335 (1995).
[2] A. Provata and G. A. Tsekouras, Phys. Rev. E **67**, 056602 (2003).
[3] G. A. Tsekouras and A. Provata, Phys. Rev. E **65**, 016204 (2001).
[4] A. Provata, G. Nicolis, and F. Baras, J. Chem. Phys. **110**, 8361 (1999).
[5] J. S. Nicholas and P. Hogeweg, Proc. R. Soc. London, Ser. B **265**, 25 (1998).
[6] W. S. C. Gurney, A. R. Veitch, I. Cruichshank, and G. Mcgeachin, Ecology **79**, 2516 (1998).
[7] J. D. Murray, *Mathematical Biology* (Springer-Verlag, Berlin, 1993).
[8] R. M. Anderson and R. M. May, Nature (London) **318**, 323 (1985).
[9] R. M. Anderson and R. M. May, Science **215**, 1053 (1982).
[10] U. Dieckmann, R. Law, and J. A. J. Metz, *The Geometry of Ecological Interactions: Simplifying Spatial Complexity* (Cambridge University Press, Cambridge, England, 2000).
[11] J. A. Sherratt, B. T. Eagan, and M. A. Lewis, Philos. Trans. R. Soc. London, Ser. B **352**, 21 (1997).
[12] Jörg R. Weimar and Jean-Pierre Boon, Phys. Rev. E **49**, 1749 (1994).
[13] B. T. Grenfell, O. N. Bjørnstad, and J. Kappey, Nature (London) **414**, 716 (2001).
[14] D. A. T. Cummings, N. E. Huang, T. P. Endy, A. Nisalak, and B. D. S. K. Ungchusak, Nature (London) **427**, 344 (2004).
[15] T. Antal, M. Droz, A. Lipowski, and G. Ódor, Phys. Rev. E **64**, 036118 (2001).
[16] M. Droz and A. Pekalski, Physica A **298**, 545 (2001).
[17] W. M. van Ballegooijen and M. C. Boerlijst, Proc. Natl. Acad. Sci. U.S.A. **101**, 18246 (2004).
[18] L. F. Olsen and W. M. Schaffer, Science **249**, 499 (1990).
[19] B. T. Grenfell, A. Kleczkowski, S. P. Ellner, and B. M. Bolker, Philos. Trans. R. Soc. London, Ser. A **348**, 515 (1994).
[20] S. Djebali, Nonlinear Anal.: Real World Appl. **2**, 417 (2001).
[21] A. Vecchio, L. Primavera, and V. Carbone, Phys. Rev. E **73**, 031913 (2006).
[22] J. A. Sherratt, Physica D **95**, 319 (1996).
[23] J. D. E. David, P. Rohani, M. B. Benjamin, and B. T. Grenfell, Science **287**, 667 (2000).
[24] M. P. Hassell, H. N. Comins, and R. M. May, Nature (London) **353**, 255 (1991).
[25] P. Rohani and O. Miramontes, Proc. R. Soc. London, Ser. B **260**, 335 (1995).
[26] G. Szabó and A. Szolnoki, Phys. Rev. E **65**, 036115 (2002).